



Synthesis, microstructural characterization and optical properties of undoped, V and Sc doped ZnO thin films

P. Amézaga-Madrid, W. Antúnez-Flores, J.E. Ledezma-Sillas, J.G. Murillo-Ramírez, O. Solís-Canto, O.E. Vega-Becerra, R. Martínez-Sánchez, M. Miki-Yoshida*

Centro de Investigación en Materiales Avanzados S.C. and Laboratorio Nacional de Nanotecnología, Miguel de Cervantes 120, Chihuahua, Chih., C.P. 31109, Mexico

ARTICLE INFO

Article history:

Received 6 July 2010

Received in revised form 5 January 2011

Accepted 7 January 2011

Available online 14 January 2011

Keywords:

Thin films

Vapour deposition

Scanning and Transmission Electron

Microscopy

X-ray Diffraction

Electronic band structure

ABSTRACT

Many semiconductor oxides (ZnO, TiO₂, SnO₂) when doped with a low percentage of non-magnetic (V, Sc) or magnetic 3d (Co, Mn, Ni, Fe) cation behave ferromagnetically. They have attracted a great deal of interest due to the integration of semiconducting and magnetic properties in a material. ZnO is one of the most promising materials to carry out these tasks in view of the fact that it is optically transparent and has n or p type conductivity. Here, we report the synthesis, microstructural characterization and optical properties of undoped, V and Sc doped zinc oxide thin films. ZnO based thin films with additions of V and Sc were deposited by the Aerosol Assisted Chemical Vapour Deposition method. V and Sc were incorporated separately in the precursor solution. The films were uniform, transparent and non-light scattering. The microstructure of the films was characterized by Grazing Incidence X-ray Diffraction, Scanning Electron Microscopy, and Scanning Probe Microscopy. Average grain size and surface rms roughness were estimated by the measurement of Atomic Force Microscopy. The microstructure of doped ZnO thin films depended on the type and amount of dopant material incorporated. The optical properties were determined from specular reflectance and transmittance spectra. Results were analyzed to determine the optical constant and band gap of the films. An increase in the optical band gap with the content of Sc dopant was obtained.

© 2011 Elsevier B.V. All rights reserved.

1. Introduction

ZnO is a technologically important low-cost, environment-friendly semiconductor material. Due to its interesting properties, such as: large band gap (~3.3 eV), high transmittance, excellent thermal stability and n or p conductivity [1]; it can be applied in many areas, for example: in catalysis, optoelectronic and photoelectrochemical devices [2]. Furthermore, this semiconductor exhibits ferromagnetic behaviour when doped with low percentages of magnetic 3d or non-magnetic cations [3]. This phenomenon is observed in thin films and nanocrystals, but not in well-crystallized bulk material. ZnO is an excellent candidate for a diluted magnetic oxide at room temperature [4]. Recently, this material has been the object of intensive investigations due to the integration of semiconducting and magnetic properties in one material that is a prerequisite for successful fabrication of useful devices for the emerging technologies of spin-electronics [5]. Works on vanadium and scandium doped zinc oxide have been scarce. ZnO:V shows ferromagnetism above room tempera-

ture upon electron doping [6–9]. On the other hand, ZnO:Sc films had better electrical and optical properties than other materials like ZnO:Al [10]. In the literature there are reports on ZnO:V and ZnO:Sc films which were deposited either by pulsed laser deposition (PLD) technique [8], a reactive plasma in a direct-current magnetron sputtering system [9,11], by standard ceramic double sintering method [12], and by sol-gel route [13]. In this work, we report a study of structural and optical properties of undoped, V and Sc doped ZnO films grown onto borosilicate glass, silicon, and sapphire substrates, using Aerosol Assisted Chemical Vapour Deposition (AACVD) method [14]. The microstructure of the films was characterized by Grazing Incidence X-ray Diffraction (GIXRD), Scanning Electron Microscopy (SEM) and Atomic Force Microscopy (AFM). The optical properties were analyzed to determine the optical constant and band gap of the films. Preliminary magnetic properties evaluation shows some degree of magnetization in Sc doped ZnO thin films, these results will be reported elsewhere.

2. Experimental

Undoped, Sc and V doped ZnO films were grown onto borosilicate 7059 glass, silicon and sapphire substrates (2.5 × 2.5 cm²), using an Aerosol Assisted Chemical Vapour Deposition set up similar to that previously reported [14,15]. The starting

* Corresponding author. Tel.: +52 614 4391114; fax: +52 614 4394884.
E-mail address: mario.miki@cimav.edu.mx (M. Miki-Yoshida).

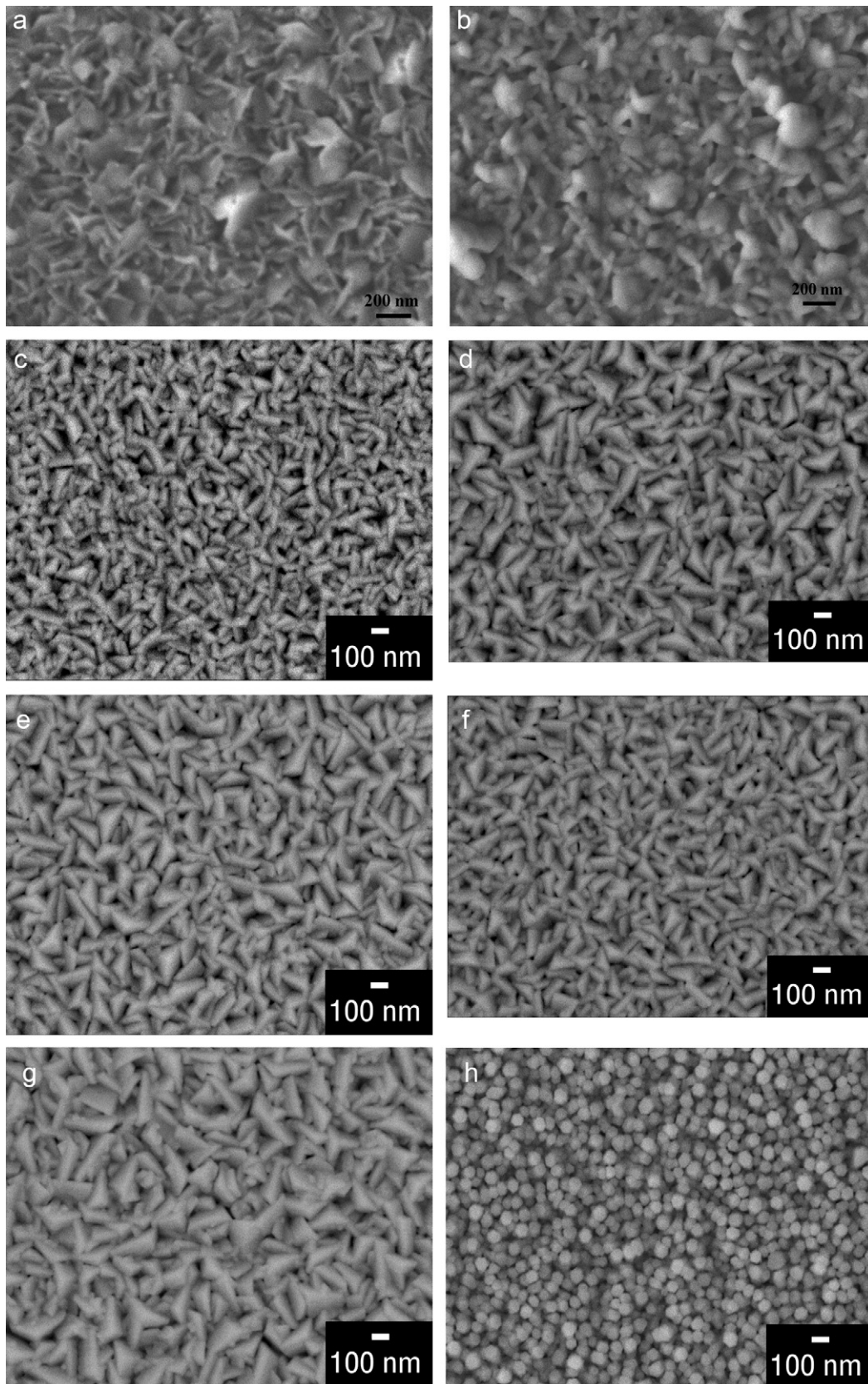


Fig. 1. Secondary electron SEM micrographs of ZnO based thin film. (a) undoped deposited at 623K; (b) undoped deposited at 673 K. Sc doped with Sc/Zn at. ratio 0.20 and different deposition time (c) B1d 39 min; (d) B1e with 57 min; (e) B1f with 69 min. Sc doped with different Sc/Zn at. ratio (f) B1g – Sc/Zn at. ratio 0.17; (g) B1h – Sc/Zn at. ratio 0.12; and (h) V doped A2j with V/Zn at. ratio 0.15.

Table 1
Principal deposition parameters of samples analyzed in this work. It is also tabulated dopant X/Zn at.% in solution and in film; substrate temperature T_s ; type of substrate; deposition time t ; surface rms roughness; films' thickness; and average grain size from SEM images.

Sample A or B = ZnO 1 = Sc2 = V	X/Zn at.% in solution	X/Zn at.% in film	T_s (K)	Substrate	Deposition time t (min)	Roughness R_{rms} (nm)	Thickness e (nm)	Grain size (SEM) (nm)
A	0	0	623	BSG	31	–		200
A2i	15	7.8 ± 1.0	623	BSG	32	3.8 ± 0.5		50
A2j	15	1.7 ± 1.5	623	BSG	50	7.2 ± 0.7	159 ± 5	75
A2k	11	3.5 ± 2.8	623	BSG	32	–		30
A2l	13	8.4 ± 2.0	623	BSG	33	3.4 ± 0.4		
A2m	13	1.6 ± 1.9	623	Silicon	33	2.4 ± 0.4		
A2n	13	1.5 ± 0.9	623	Sapphire	33	6.7 ± 0.8		
B	0	0	673	BSG	31	31 ± 2	223 ± 5	230
B1c	24	7.0 ± 0.3	723	BSG	25	5.6 ± 0.5	211 ± 5	100
B1d	20	6.5 ± 1.7	673	BSG	39	–	216 ± 5	115
B1e	20	7.3 ± 0.8	673	BSG	57	–	450 ± 5	150
B1f	20	7.6 ± 0.2	673	BSG	69	–	462 ± 5	150
B1g	18	5.3 ± 0.6	673	BSG	44	–	270 ± 5	
B1h	12	4.3 ± 0.3	673	BSG	44	–	415 ± 5	200

solutions were dilutions of zinc acetate and vanadium (III) 2,4-pentanedionate in methanol (99.9% pure), and zinc acetate and scandium (III) 2,4-pentanedionate hydrate in tri-distilled water. V and Sc concentrations in solution were varied between 0 (for undoped) to 15 at.% and 20 at.%, respectively. The films were prepared at different temperatures between 523 and 723 K. An ultrasonic nebulizer (PG-241) working at 2.4 MHz generated the aerosol that was conveyed by the carrier gas and directed towards the substrate by a nozzle, which had a periodic movement at constant velocity (~ 1 cm min^{-1}) to scan the whole surface of the substrate. The total number of steps was varied in order to obtain films of different thickness. Optimum parameters were determined and kept constant in all the samples reported in this work. The most important conditions were: optimum temperature between 623 and 673 K, carrier gas (air or nitrogen) flow of 5 L min^{-1} , distance from the nozzle to the substrate of 1 mm, concentration of precursor solution adjusted to 0.1 mol L^{-1} , independent of the ratio X/Zn, where X is the dopant. Table 1 summarizes the principal deposition parameters used in this work.

The surface morphology and film's thickness were studied by field emission SEM using a JEOL JSM-7401F operated at 7 kV. To determine the thickness, cross sectional samples of the films were observed. Elemental microanalysis of the films was achieved by Energy Dispersive X-ray Spectroscopy, using an Inca microanalysis system attached to the electron microscope. GIXRD patterns were acquired to determine the crystalline phases present in the films. They were obtained in a Pan-analytical X-Pert system, using Cu $K\alpha$ radiation ($\lambda = 0.15418$ nm) at 40 keV and 35 mA. Grazing incidence angle was fixed at 0.5° and scanning angle 2θ was varied between 25° and 90° , at 0.02° step. AFM images were obtained using a Multimode Nanoscope IVa SPM apparatus (Veeco) recorded in tapping mode using commercial n-type standard silicon cantilever (model TESP, Veeco) with spring constant 20 N/m. Surface rms roughness were estimated from measurement of several AFM images of the films. Optical properties, in the range between 300 and 1100 nm, were determined from specular reflectance (at an angle less than 7° from the normal to the surface), and transmittance spectra in a Perkin Elmer Lambda 35 spectrophotometer.

Table 2
Peak position (2θ), experimental FWHM, peak broadening B , average crystallite size (nm), experimental interplanar distance d_{EXP} (nm), lattice parameters a (nm) and c (nm) of undoped, Sc and V doped ZnO films. For this ($30 < 2\theta < 39$) interval, instrumental broadening was estimated $\sim 0.04^\circ$, from diffraction pattern of Si standard.

Sample	Peak position (2θ)	FWHM exp.	Peak broad. B	Average crystallite size (nm)	d_{EXP} (nm)	a (nm)	c (nm)
A	31.95	0.37	0.33	25 ± 1	0.2799 ± 0.0003	0.3232 ± 0.0003	0.5178 ± 0.0001
	34.62	0.37	0.33		0.2589 ± 0.0003		
	36.45	0.36	0.32		0.2463 ± 0.0003		
A2j	31.83	0.18	0.14	40 ± 17	0.2809 ± 0.0003	0.3242 ± 0.0003	0.5178 ± 0.0001
	34.61	0.29	0.25		0.2590 ± 0.0003		
	36.41	0.35	0.31		0.2466 ± 0.0003		
A2k	34.63	0.44	0.4	20 ± 1	0.2588 ± 0.0003	0.3240 ± 0.0003	0.5177 ± 0.0001
	36.37	0.46	0.42		0.2468 ± 0.0003		
A2m	34.61	0.36	0.32	23 ± 5	0.2590 ± 0.0003	0.3234 ± 0.0003	0.5180 ± 0.0001
	36.44	0.48	0.44		0.2464 ± 0.0003		
B	31.92	0.36	0.32	24 ± 3	0.2801 ± 0.0003	0.3233 ± 0.0004	0.5173 ± 0.0005
	34.64	0.44	0.40		0.2587 ± 0.0003		
	36.49	0.36	0.32		0.2460 ± 0.0003		
B1d	31.89	0.42	0.38	20 ± 2	0.2804 ± 0.0003	0.3239 ± 0.0004	0.5192 ± 0.0005
	34.53	0.46	0.42		0.2595 ± 0.0003		
	36.34	0.52	0.48		0.2470 ± 0.0003		
B1e	31.90	0.38	0.34	21 ± 3	0.2803 ± 0.0003	0.3238 ± 0.0004	0.5197 ± 0.0005
	34.49	0.43	0.39		0.2598 ± 0.0003		
	36.34	0.52	0.48		0.2470 ± 0.0003		
B1f	31.91	0.42	0.38	21 ± 3	0.2802 ± 0.0003	0.3235 ± 0.0004	0.5195 ± 0.0005
	34.51	0.4	0.36		0.2597 ± 0.0003		
	36.36	0.51	0.47		0.2469 ± 0.0003		
B1g	31.93	0.4	0.36	21 ± 2	0.2801 ± 0.0003	0.3235 ± 0.0004	0.5189 ± 0.0005
	34.55	0.46	0.42		0.2594 ± 0.0003		
	36.39	0.47	0.43		0.2467 ± 0.0003		
B1h	31.92	0.36	0.32	22 ± 3	0.2801 ± 0.0003	0.3236 ± 0.0004	0.5188 ± 0.0005
	34.55	0.44	0.40		0.2594 ± 0.0003		
	36.40	0.45	0.41		0.2466 ± 0.0003		

3. Results and discussion

3.1. Structural properties

Films were polycrystalline, uniform, transparent and non-light scattering. Fig. 1a and b shows secondary electron SEM micrographs of typical surface morphology of undoped ZnO thin films. Fig. 1a shows the surface morphology of sample A prepared at 623 K and Fig. 1b shows sample B prepared at 673 K. Samples A and B were prepared as a reference, to be compared with doped samples. Typical hexagonal flake like grains were observed. As expected, it shows an increase of the grain size when the deposition temperature increases.

For doped samples, substrate temperature was varied between 523 and 723 K, in order to determine its optimum value, to introduce uniformly the dopant. It was found that dopant content of the film decreased as the substrate temperature increased; however for temperatures below 623 K, incomplete dopant precursor salt decomposition occurs, giving rise to the presence of organic residues in the films. As a consequence, optimum substrate temperatures of 673 and 623 K was deduced for Sc and V doped films, respectively.

Sc doped ZnO samples present similar surface morphology and grain size. Fig. 1c–e, shows SEM micrographs of ZnO:Sc samples B1d, B1e and B1f, respectively. In this case, the samples were prepared at 673 K, with the same Sc/Zn = 0.20 at. ratio in solution, but different deposition time (number of deposition cycles) and consequently different film thickness. Here also, a minor increase of the grain size with the deposition time was observed (see Table 2), consistent with XRD results (see below). EDS analysis was performed in several zones of the films, at low magnification ($\sim 300\times$), to check dopant distribution uniformity. It was determined that Sc/Zn at. ratio in the films was $\sim 0.071 \pm 0.009$, with a slight tendency to increase with deposition time (see Table 1). Thus, taking as a reference Zn contents, only around 35% of the dopant in solution was deposited into the film. From these results, at the optimum substrate temperature (673 K), it can be concluded that Sc was distributed uniformly throughout all the ZnO film. Additionally, the dopant content was almost the same despite increasing deposition time. In comparison to undoped sample (B) (Fig. 1b) obtained at the same temperature, doped samples show a marked texture (see Fig. 2a) then crystallites show similar orientation respect to the surface of the sample. Other samples with lower Sc content were deposited at the same optimum temperature (see Table 1). Fig. 1f and g shows secondary electron SEM micrographs of samples B1g and B1h, prepared with different Sc/Zn at. ratio in solution of 0.18 and 0.12, respectively. Sc/Zn at. ratio in film B1g was 0.053 ± 0.006 ; whereas for sample B1h it was 0.043 ± 0.003 . For these films, the same general conclusions can be made: Sc dopant was uniformly distributed, only around 33% of the dopant in solution goes into the film (with reference to Zn content), and a minor increase of the grain size with the decrease of dopant concentration was observed, consistent with XRD results (see below). Samples deposited using nitrogen as the carrier gas were less uniform and Sc/Zn at. ratio was lower than that in films deposited with air.

On the other hand, V doped ZnO thin films were prepared at 623 K, with V/Zn at. ratio around 0.15 in solution. Fig. 1h presents the typical morphology of V doped samples. In contrast to undoped films, V doped ZnO samples present a very different surface morphology and grain size. Grains appear as small hexagonal rods, less than 100 nm wide and long, grown normal to the substrate. This abrupt change was probably generated by a modification of the interfacial energies of the constituent solids (substrate, film), adsorbed reactants at the surface and precursor gasses. Similar to the case of Sc doped films, a minor increase of the grain size with the deposition time was observed. However unexpectedly,

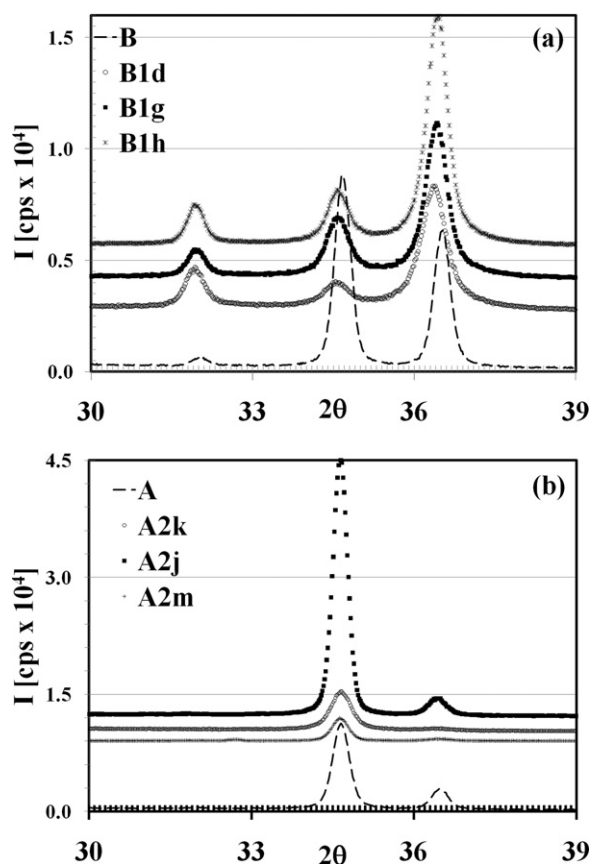


Fig. 2. GIXRD patterns of doped ZnO films with different dopant content, in comparison with corresponding undoped sample (A or B). (a) Sc doped films (B1d – Sc/Zn at. ratio 0.20; B1g – Sc/Zn at. ratio 0.17; and B1h – Sc/Zn at. ratio 0.12). (b) V doped films (A2j – V/Zn at. ratio 0.15; A2k – V/Zn at. ratio 0.11; and A2m – V/Zn at. ratio 0.13).

EDS microanalysis revealed that V/Zn at. ratio in the films present a markedly tendency to decrease with deposition time (see Table 1). Dopant distribution, in this case, was less uniform throughout all the film; it is evident if we compare the standard deviation of V/Zn at. ratio in film to that of Sc/Zn. Additionally, an appreciably grain size reduction was observed as the dopant concentration was changed.

The crystalline structure of the films was analyzed by GIXRD. All the films were polycrystalline, with a hexagonal wurtzite structure [16]. Fig. 2a shows GIXRD patterns of Sc doped ZnO films obtained at 673 K (B1d – Sc/Zn at. ratio, but different thickness (B1d, B1e, B1f), in comparison with undoped sample B. A change in the intensity of peaks can be observed, which shows a change in preferential growth direction. Lattice parameters were calculated from the position of principal diffraction peaks (1 0 0), (0 0 2) and (1 0 1). For undoped films, values of parameters “a” and “c”, are lower than bulk values; evidencing the existence of structural strain in the films (see Table 2). For Sc doped films, both parameters are higher ($\Delta a \sim 0.0003$; $\Delta c \sim 0.002$) than undoped sample B, but still lower than bulk values [16]. For samples B1d, B1e and B1f, and increase of “c” and a decrease of “a” is observed as the films’ thickness increases; this fact indicates a compression stress parallel to the basal plane of the hexagonal structure. Additionally, as the Sc/Zn ratio decreases in samples B1g and B1h, lattice parameters decrease towards that of undoped samples.

Fig. 2b shows GIXRD patterns of V doped ZnO samples, in comparison to undoped sample A obtained at the same temperature 623 K. It also shows a change in the intensity of the diffracted lines, doped samples present a predominance of (0 0 2) peak. In this case

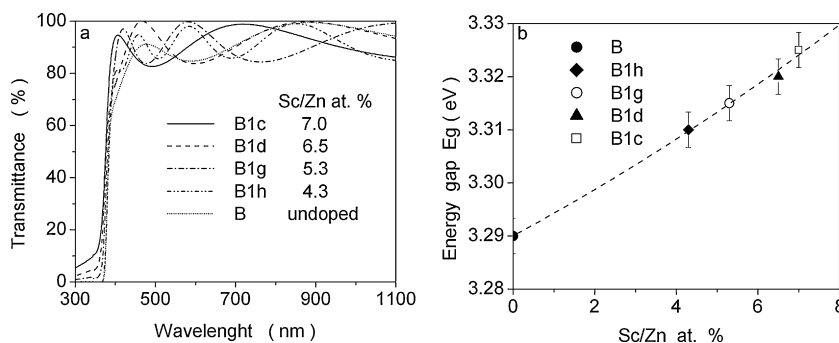


Fig. 3. (a) Optical transmission spectra for the undoped and doped ZnO thin films prepared with different content of Sc. (b) Energy gap of the ZnO thin films as a function of the content of Sc. The dash line represents a parabolic fitting to the calculated data, only for eye-guide.

again, lattice parameters “*a*” and “*c*” are lower than those of undoped films (see Table 2).

Instrumental broadening around the (100), (002) and (101) peaks of ZnO was measured using a Si standard, we have obtained a peak broadening of 0.04° . Correcting the experimental FWHM of the diffraction peaks with the instrumental broadening, and assuming no strain broadening, crystallite size was estimated by Scherrer's equation [17]. The crystallite size of Sc doped films was smaller than that of undoped ZnO sample. Consistent with SEM results crystallite size slightly increased with deposition time (see Table 2). As it is known, grain size by SEM measurement gives a morphological estimation; in contrast, crystallite size obtained by XRD gives the dimension parallel to the scattering vector. Thus, both values do not necessarily coincide. Table 2 presents the average crystallite size, interplanar distance and other quantities obtained from the analysis of GIXRD patterns, of representative samples.

Atomic Force Microscopy was used to measure the surface roughness of representative films. There is a drastic decrement in surface roughness for the doped sample, indistinctly for V or Sc doped films (see Table 1). Grain size and morphology were similar to SEM images.

3.2. Optical properties

An average transmittance of above 90% in the visible range was obtained in both ZnO:Sc and ZnO:V thin films. As a representative example, Fig. 3a shows the transmission spectra of ZnO:Sc thin films prepared with different Sc content, maintaining constant the deposition temperature, except for B1c sample. Increasing the Sc content in the film, a shift to higher energies (blue shift) of the absorption edge in the transmittance spectrum can be observed in Fig. 3a. This shift is mainly attributed to the Burstein–Moss effect, resulting from the increase of carrier concentration.

The optical constants, i.e. refractive index *n* and extinction coefficient *k* were determined from transmittance and reflectance spectra as in Ref. [18] and employing TFCalc 3.5.14 software. The refractive index of the ZnO based thin films was in the range of 1.990 at 300 nm to 1.935 at 1100 nm having an average value of 2.019 at the center of the visible range, 550 nm. The average extinction coefficient for several representative ZnO films had a relevant value only close to the absorption edge, around 350 nm. In the visible range and at the beginning of near infrared range, from 400 to 1100 nm, the extinction coefficient was taken as zero.

The absorption coefficient as a function of wavelength was determined, from measurements of transmittance and reflectance spectra. Then, the absorption coefficient was utilized to obtain another optical parameter of great relevance, the band gap energy. The band gap was estimated using the Tauc's relationship between

the absorption coefficient α , and the photon energy $h\nu$, using:

$$\alpha h\nu = A \times (h\nu - E_g)^n$$

where *A* is an energy independent constant, E_g , is the optical band gap and *n* is a constant which determines the type of the optical transition ($n = 1/2$ for direct allowed transitions, and $n = 2$ for indirect transitions). We assume in our case a direct allowed transition. The values of the direct band gap (E_g) can be obtained, when the straight portion of $(\alpha h\nu)^2$ against $h\nu$ plot is extrapolated to 0. The optical band gap energy of ZnO:Sc thin films increased as the Sc content increased, from 3.29 eV for the undoped sample to around 3.32 eV for film B1c (Sc/Zn at. ratio = 0.07), as shown in Fig. 3b. The impurity content-dependence of the energy gap of ZnO:Sc films is apparently sublinear for the interval of Sc content considered here. From the results described above, it can be concluded that Sc is a dopant for producing high transparent ZnO thin films with controllable band gap energy.

4. Conclusion

High quality, polycrystalline with a hexagonal wurtzite structure, uniform, highly transparent and non-light scattering ZnO based thin films were deposited by Aerosol Assisted Chemical Vapour Deposition method. In order to introduce uniformly adequate quantities of the dopants, an optimum substrate temperatures of 673 and 623 K were deduced for Sc and V doped films, respectively. At optimum substrate temperatures, Sc doped films were more uniform. Lattice parameters of doped and undoped samples, were lower than those reported in reference [16]. In general, crystallite and grain size of the doped samples were smaller than those of undoped films. The optical band gap, obtained from transmittance and reflectance spectra of ZnO:Sc thin films, increased as the Sc content increased, from 3.29 eV for the undoped sample to around 3.32 eV for film B1c (Sc/Zn at. ratio = 0.07).

Acknowledgements

The authors would like to thank K. Campos, J. Sáenz, E. Torres, C. Ornelas, S. Miranda, and M. Moreno for experimental assistance. This work was partially supported by a grant from SEP-CONACYT project N°CB-2008-01-106655 and FONCICYT project N° C0002-2008-01-94682.

References

- [1] T. Yamamoto, Thin Solid Films 106 (2002) 420–421.
- [2] M. Deepa, N. Bahadur, A.K. Srivastava, P. Chaganti, K.N. Sood, J. Phys. Chem. Solids 70 (2009) 291–297.
- [3] J.M.D. Coey, Curr. Opin. Solid State Mater. Sci. 10 (2006) 83–92.
- [4] T. Dietl, H. Ohno, F. Matsukura, J. Cibert, D. Ferrnad, Science 287 (2000) 1019.

- [5] J.F. Gregg, I. Petej, E. Jouguelet, C. Dennis, *J. Phys. D: Appl. Phys.* 35 (2002) R121–R155.
- [6] N.H. Hong, J. Sakai, A. Hassini, *J. Appl. Phys.* 97 (2005) 10D312.
- [7] Y. Ishida, J.I. Hwang, M. Kobayashi, A. Fujimori, H. Saeki, H. Tabata, T. Kawai, *Physica B* 351 (2004) 304.
- [8] H. Saeki, H. Tabata, T. Kawai, *Solid State Commun.* 120 (2001) 439.
- [9] M. Faiz, N. Tabet, A. Mekki, B.S. Mun, Z. Hussain, *Thin Solid Films* 515 (2006) 1377–1379.
- [10] T. Minami, T. Yamamoto, T. Miyata, *Thin Solid Films* 366 (2000) 63–68.
- [11] C. Miao, Z. Zhao, X. Ma, Z. Ma, *Physica B*, doi:10.1016/j.physb.2010.05.087.
- [12] R. Krithiga, G. Chandrasekaran, *J. Cryst. Growth* 311 (2009) 4610–4614.
- [13] R. Sharma, K. Sehrawat, A. Wakahara, R.M. Mehra, *Appl. Surf. Sci.* 225 (2009) 5781–5788.
- [14] P. Amézaga-Madrid, W. Antúnez-Flores, I. Monárrez-García, J. González-Hernández, R. Martínez-Sánchez, M. Miki-Yoshida, *Thin Solid Films* 516 (2008) 8282–8288.
- [15] P. Amézaga-Madrid, W. Antúnez-Flores, R.J. Sáenz-Hernández, R. Martínez-Sánchez, M. Miki-Yoshida, *J. Alloys Compd.* 483 (2009) 410–413.
- [16] Joint Committee on Powder Diffraction Standards, *Powder Diffraction File*, International Center for Diffraction Data, Swarthmore, PA, 2006, card 00-036-1451.
- [17] B.D. Cullity, S.R. Stock, *Elements of X-Ray Diffraction*, 3rd edition, Prentice Hall, New Jersey, 2001, p. 170.
- [18] C. Gumus, O.M. Ozkendir, H. Kavak, Y. Ufuktepe, *J. Optoelectron. Adv. Mater.* 8 (2006) 299–303.